JOURNAL OF MATERIALS SCIENCE 26 (1991) 4765–4773

Fatigue properties of wood in tension, compression and shear

P. W. BONFIELD, M. P. ANSELL
School of Materials Science, University of Bath, BA2 7AY, UK

The fatigue properties of wood laminates have been investigated in tension, compression and shear. Fatigue lives in compression are significantly less than in tension, and S–N data at five R ratios has yielded a set of constant-life lines, the form of which is related to the failure mode of the wood observed by scanning electron microscopy. A point of inflection in the constant-life lines at the transition between all compressive and partially tensile fatigue loading is a new observation. S–N curves for wood laminates have been produced for shear across the radial–longitudinal and tangential–longitudinal planes, and the latter plane is observed to be more resistant to fatigue loads. Samples with four times the cross-sectional area of standard-sized samples have been fatigued at $R = -1$ and no significant difference in fatigue life is apparent. It appears that the absence of a size effect in tension–compression results from the orthotropic structure of wood which is insensitive to variations in the density of surface flaws.

1. Introduction

The fatigue properties of wood in flexure have been reported in a recent paper [1]. The fatigue results were produced in response to the needs of the UK wind-power industry which had noted the successful use of laminated wood in wind turbine blades in the USA. The flexural fatigue programme generated S–N curves at several moisture contents and R ratios (ratio of minimum to maximum stress under sinusoidal loading), produced constant-life lines and established mechanisms of fatigue damage accumulation in wood.

Whilst the results of flexural fatigue testing are appropriate to wooden wind turbine blades, especially close to the blade root, it is clear that the outer surfaces of large wind turbine blades experience predominantly tensile or compressive loads, as the blades are hollow structures. The construction is usually a D-spar incorporating a wood or composite shear web bonded at right angles to the laminated wood blade faces.

The static flexural, tensile, compressive and shear strengths of wood are widely different because the mechanisms of failure in each loading configuration, (e.g., buckling in compression and cell extension in tension), is influenced by wood's cellular structure. The UK Department of Energy, which has funded this research, has considered it necessary to investigate thoroughly the fatigue properties of wood laminates in tension, compression and shear to complement the flexural results which have already been reported. This has involved the use of two 20-tonne capacity fatigue machines with hydraulically operated wedge grips, whereas the flexural work was performed with a 0.5 tonne actuator.

A further preoccupation is the effect of size on the fatigue life of wood. The detrimental effect on strength of increasing sample size has already been reported [2, 3] or suggested [4] for wood in static flexure, but it is not clear whether these effects are evident in axial fatigue. As wind turbine blades become larger, it is important to establish whether such a size effect will impose a penalty on the use of laminated wood in thick sections.

This paper provides an update of the wood fatigue literature, and presents S–N data for laminated wood in tension/compression and shear. The tension/compression results at various R ratios have been combined to produce a set of constant life lines for fatigue design purposes and these are compared with earlier flexural results. Laminated wood samples with four times the cross-sectional area of standard samples have been loaded in axial fatigue to investigate the possible occurrence of a size effect. Finally the fracture topographies of wood fatigued in tension, compression, tension/compression and shear have been observed by electron microscopy to establish the link between loading mode and structural response.

2. Literature review

The wood fatigue literature has already been extensively reviewed [1] in this journal. Since then NASA/DOE reports have appeared in the literature which present results on axial fatigue in wood, which is the concern of this paper. These reports are reviewed below.

The static and fatigue properties of a Douglas fir/epoxy laminated wood composite material were investigated [5] for use as the primary material for the blades of the NASA/DOE MOD 5A wind turbine. The work was divided into two main sections which were the development of suitable sample geometries and the generation of both static and fatigue baseline

0022–2461/91 $03.00 + .12

data. Problems arose in the design of a suitable gripping arrangement and sample geometry for the fatigue tests. After evaluating fourteen different arrangements, a successful geometry was developed using a dog-bone shaped sample. U-shaped crush limiters were used to avoid crushing of tensile samples in the test machine hydraulic wedge grips.

In the longitudinal direction a mean tensile strength of 100.4 MPa with a mean tensile Young's modulus of 17.5 GPa and a mean compressive strength of 67.7 MPa and a mean compression modulus of 15.0 GPa were obtained for Douglas fir laminates at room temperature. Fatigue tests were carried out for jointed and unjointed samples at room temperature and "room humidity" and at 49 °C and 100% relative humidity. R ratios of 0.0, -0.5 and -1 were used for the room temperature and humidity samples and 0.0 and -1 for the 49 °C and 100% relative humidity tests. The inherent variability of wood was demonstrated with up to three orders of magnitude variation in life. This scatter caused difficulty in determining the effect on fatigue life of (a) the presence of joints and (b) increasing the humidity and temperature. It was concluded that further testing and statistical analysis were necessary to determine if these variables have a statistically significant effect. All tests were carried out at 5 Hz so that no allowance was made for the rate dependence of the properties of wood. The results are difficult to interpret because of the scarcity and scatter of points on the S–N plots.

The results of exploratory fatigue tests on Douglas fir/epoxy laminates augmented with layers of carbon fabric have been reported [6]. The aim was to try and increase the modulus of the bulk laminate around the steel stud fixings used to attach the blade to the hub of the wind turbine and so improve the load take-off from the steel to the wood laminate. Static and fatigue compression and tensile tests were carried out on fully augmented, partially augmented and non-augmented samples at room temperature, -11 °C and -40 °C. An R ratio of 0.1 was used for the tension tests and $R=10$ for the compression tests. Augmenting the wood laminate improved fatigue performance but large scatter in fatigue life was observed and S–N curves produced in compression were notably flat.

The effect of scarf joint geometry on the static and fatigue performance of Douglas fir/epoxy laminates in compression was investigated in the same report [6]. A comparison of the performance of scarfs with slopes of 4:1, 10:1, 16:1, and no scarf joints was made. It was found that the scarf joints with shallow slopes performed better than joints with steeper slopes, especially in fatigue. Laminate joining faults, such as gaps or incomplete overlaps, affected compressive properties, but fairly substantial overrides had a minimal effect when compared to perfect scarf joints.

Cantilever beam fatigue tests have been used to assess the fatigue life of wind turbine blade root-ends [7]. A qualitative assessment of the performance of several materials combinations was carried out. Laminated wood, low-cost steel, fibreglass and aluminium blade materials were all tested and compared. It was found that the cantilever beam type of fatigue test was useful in this qualitative test process but no conclusions were drawn relating to the relative merits of these materials.

The use of studs for blade-root-to-hub attachment has been investigated [8]. Static and fatigue tests were performed on Douglas fir and ash with studs bonded into them, and a 6 m long blade section mounted as a cantilever beam in flapwise and edgewise orientations was also tested. It was concluded that the bonded in studs performed statisfactorily and with a positive margin of safety.

In summary it appears that most of the NASA/DOE wood fatigue research is concerned with joints and stud fixings. Axial S–N fatigue results are sparse and lack statistical validity, indicating the need for a comprehensive evaluation of wood laminates over a broad range of R ratios at a standardized rate of stress application.

3. Experimental procedure

3.1. Fatigue equipment

Two Mayes 20-tonne servohydraulic machines were used for fatigue testing and ramp loading. One fatigue frame has only two supporting columns and is mounted on a 2 m long steel bed plate. This arrangement allows the fatigue frame to be moved backwards and forwards through slots along the bed plate and enables either large flexural samples, or cantilever-mounted samples (for example blade roots) to be tested. As a result the fatigue frame has most of its hydraulic components mounted on top of the crosshead.

The second Mayes machine is a more conventional four-column machine with a 1.8 m long raised and slotted bed plate. The wedge boxes can be fitted with one of two sets of wedge grips, allowing samples of between 20 and 30 mm or 30 and 40 mm in thickness to be gripped. A strain module has been included in the control panel of this machine to condition signals from an extensometer of variable gauge length. Both machines can be load, position or displacement controlled, and the value of the other two parameters determined in each control mode. The second machine can, in addition, be strain controlled.

The actuators are provided with hydraulic power from a high-capacity power pack, consisting of four electric motors which drive four pumps, each capable of pumping up to 45 litres/minute of oil. The hydraulic power system has a ring main configuration to serve both fatigue actuators and each fatigue frame can be controlled independently using saw-tooth, sinusoidal or square waveforms. For low-frequency tests, ramp tests or creep tests an integral action facility is used which ensures that desired loads are achieved and held. Test rates of up to 9000 cycles per minute can be maintained. The clamping pressure of the hydraulic wedge grips is adjustable.

3.2. Materials

The major material used by British manufacturers of commercial wind turbines in the construction of bla-

des is 4 mm thick Khaya ivorensis veneer laminated with epoxy resin. Khaya ivorensis is an intermediate density ($\sim 450\,kg\,m^{-3}$) African mahogany that is used because it is relatively cheap and readily available in thick veneer form. There is little density change in the wood due to seasonal variations because it is a tropical hardwood. It contains a high-volume proportion of vessels which allow easy passage of resin during vacuum bagging, ensuring minimum thickness glue lines in the laminated product.

As in the manufacture of wind turbine blades, the wood laminates for sample preparation are produced by laminating together 4 mm thick sheets of Khaya ivorensis, coated on each side with Structural Polymer Systems SP 110/210 room temperature cure epoxy resin, thickened by incorporating a cellulosic fibrous filler. The laminate of the required thickness is then consolidated by vacuum-bagging.

Douglas fir is a softwood used for turbine blade manufacture in the USA and by British manufacturers for the US blade replacement market. The fatigue properties of Douglas fir laminates, fabricated from 4 mm veneers, have also been investigated.

As wood is a moisture-sensitive material [1, 9] samples are conditioned at 65% relative humidity (RH) at room temperature before testing so that a moisture content of approximately 10% is achieved. During fatigue tests samples are surrounded by a plastic membrane containing baths of concentrated sodium nitrite solution so that a 65% RH environment is maintained throughout the test.

3.3. Sample geometry and gripping arrangement

The transfer of a lateral gripping load at the wedge grips into an axial load through the gauge length of a fibre-reinforced composite specimen, particularly a unidirectionally reinforced specimen, always requires careful consideration so that valid failures away from the wedge grips are achieved. The wood laminates used in this work are no exception and the susceptibility of wood to crushing under load at right angles to the grain direction poses an additional problem.

Samples were cut with dimensions of 12 mm thick (2×4 mm core plies plus 2×2 mm ply facings) by 50 mm wide by 300 mm long. They required end-tabbing and profiling in such a way that acceptable failures occurred in fatigue. A solution to the gripping problem was achieved using overlapping aluminium end tabs that had machined aluminium bar inserts glued between them at the edges. This avoided crushing of the wood between the wedge grips. Practice showed that the insertion of a sacrificial wood veneer between the aluminium tabs and the ends of the sample (Fig. 1), successfully transferred load from shear between the grips to an axial load in the gauge length of the specimen.

Necked samples were required to ensure that failure occurred away from the end tabs. The 50 mm wide samples were smoothly profiled down to a width of 30 mm over a 20 mm length in the central part of the specimen. Failure occurred within the necked centre

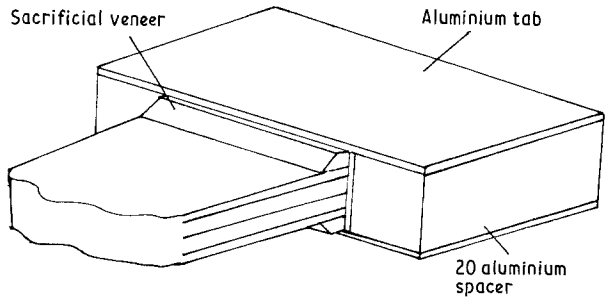

Figure 1 Gripping arrangement for tension/compression sample.

section of the specimen and the profile curvature was sufficiently shallow to prevent longitudinal cracks running along the grain into the end-tabbed region from the edges of the central neck. Furthermore, buckling in compression was prevented because a sufficiently low length-to-thickness ratio (150 mm: 12 mm) was adopted.

3.4. Shear samples

Khaya laminates were also tested in shear because, although the major stresses experience by Khaya in wind turbine blades are tensile and compressive in nature, they also experience shear loads at, for example, the blade root. There are numerous shear testing modes [10] which can be used in the laboratory. The method adopted involved loading a straight-sided specimen in tension, with offset horizontal cuts extending to half the width of the sample from opposite edges (Fig. 2). Shear failure was constrained to take place between the tips of these cuts along the central axis of the sample. Samples with the wood grain running along the specimen axis, with dimensions 12 mm by 30 mm by 300 mm, were prepared with the veneer in two orientations, namely, with the glue lines parallel to the sample face and with the glue lines parallel to the sample edge. This allowed shear testing along both the radial–longitudinal (RL) and tangential–longitudinal (TL) planes.

3.5. Visual inspection and electron microscopy

Fatigue specimens were examined visually during testing to observe the development of surface damage. At failure, fracture surfaces, sputter-coated with gold, were studied with a Jeol T330 scanning electron microscope (SEM) in order to relate the loading mode to the fracture topography.

3.6. Experimental programme

Axial ramp tests in both compression and tension were carried out on wood laminates along the longitudinal axis of the wood, using the Mayes fatigue machine with wedge grips for the tensile tests. An Instron 1195 screw-driven machine was used for the compression tests, where samples were crushed between flat platens. Some static compression tests were carried out, with the Instron, across the grain (loaded along the radial axis) so that the maximum clamping

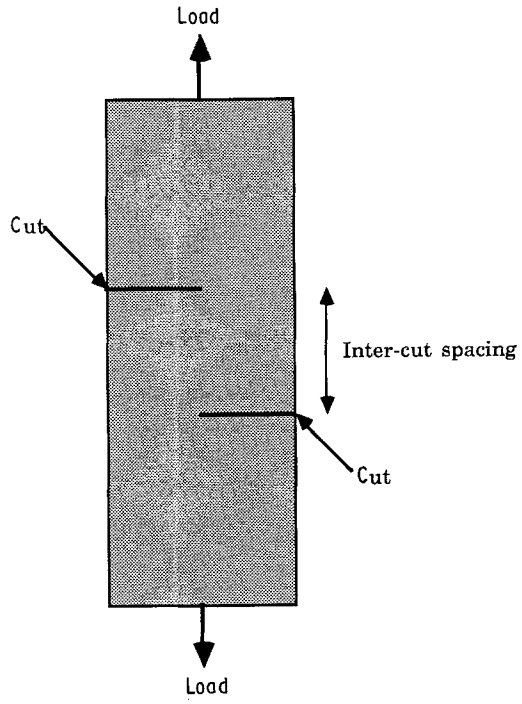

Figure 2 Shear fatigue specimen.

pressure at the hydraulic wedge grips could be calculated for size-effect samples, which did not require end tabs. The static strength of shear samples was measured for samples with a range of inter-cut distances, again using the Instron.

Constant-amplitude fatigue tests at R ratios ($\sigma_{min}/\sigma_{max}$) of 0.1, -1, -2, -10, and 10 were carried out to assess the effect of R ratio on fatigue performance. The R ratios chosen correspond to loads which are all tensile, ($R = 0.1$), mixed tensile/compressive ($R = -1$, reversed loading; -2, twice as much compression as tension; and -10, ten times as much compression as tension) and all compressive ($R = 10$). All tests were carried out at a constant rate of stress application of 200 MPa/sec which was the maximum rate that avoided adiabatic heating in the fatiguing sample. Adopting a constant strain rate eliminates strain rate related effects, although these should be minimal in axially loaded wood, and it has the advantage of speeding up low-amplitude fatigue tests which endure a corresponding high number of cycles to failure, hence making better use of machine time.

Tests at $R = -1$ have been carried out on large wooden laminate samples to establish whether a size effect is observed in axial fatigue. These scaled-up samples have a necked profile with a minimum width at their centre point of 36 mm and a thickness of 40 mm. The standard sample dimensions are 30 mm wide by 12 mm thick. The ratio of cross-sectional areas between the large and standard samples is therefore four.

S–N curves have been generated at $R = 0.1$ for samples sheared along the RL and TL planes.

4. Experimental results and discussion

4.1. Static axial and shear testing

A mean compressive strength of 49.5 $\pm$ 2.8 MPa was obtained from 32 Khaya samples. This value compares well with literature values [9] and the large amount of variation is typical for an inherently variable material such as wood. The amount of scatter was reduced as much as possible by carefully grading the wood and rejecting damaged veneers before laminating. The uniform nature of an equatorially grown wood reduces the amount of scatter in strength that might be expected in some species containing annual rings.

The mean tensile strength for Khaya was found to be 81.8 $\pm$ 9.3 MPa and again this value compares well with literature values [9]. A mean compressive strength of 12.59 $\pm$ 0.64 MPa was measured when Khaya was transversely loaded, perpendicular to the grain of the wood. The mean compressive strength of Douglas fir was found to be 61.2 $\pm$ 8.8 MPa and the tensile strength was taken to be 100.4. MPa from the literature [5].

An important consideration in the use of the shear test described in Section 3.4 is the length adopted between the horizontal cuts. A number of static tests were performed on RL shear samples of Khaya with lengths of 20 mm (8), 35 mm (11), 50 mm (8), 70 mm (8) and 100 mm (8). (The number of tests appear in parentheses). The static shear strengths are presented in Fig. 3, with the $\pm$ standard deviation at each inter-cut length. Initially the shear strength is independent of inter-cut length, but for lengths greater than 50 mm the strength falls off. It was decided, on the basis of these tests, to fatigue test in shear with an inter-cut distance of 35 mm which is at the centre of the horizontal portion of the strength plot. The static RL shear strength (9.5 $\pm$ 2.3 MPa) corresponds well with literature values [9]. A mean static shear strength of 9.5 $\pm$ 1.1 MPa was achieved for TL samples using the 35 mm inter-cut distance.

Other test geometries have been used at Bath for static shear tests on wood laminates, including lap shear and rail shear, and these have yielded similar results but with greater scatter and difficulty of testing compared with the edge-cut geometry.

4.2. Tension/compression fatigue

Maximum compressive stress versus log number of cycles-to-failure, (S–N curves), for all R ratios except

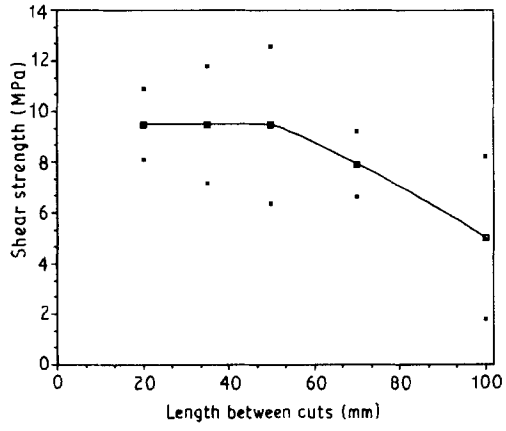

Figure 3 Shear strength versus inter-cut distance.

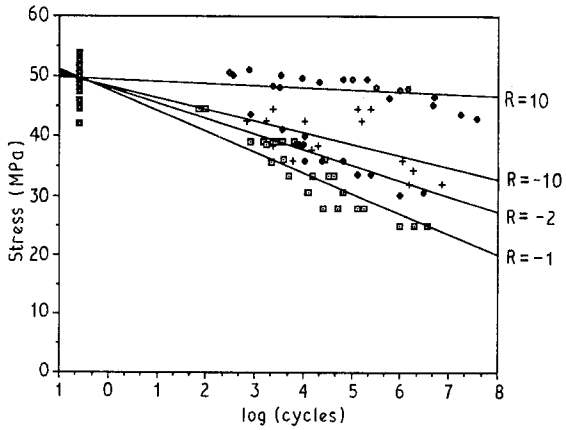

Figure 4 S–N data for Khaya axially loaded at $R = -1$, -2, -10 and 10.

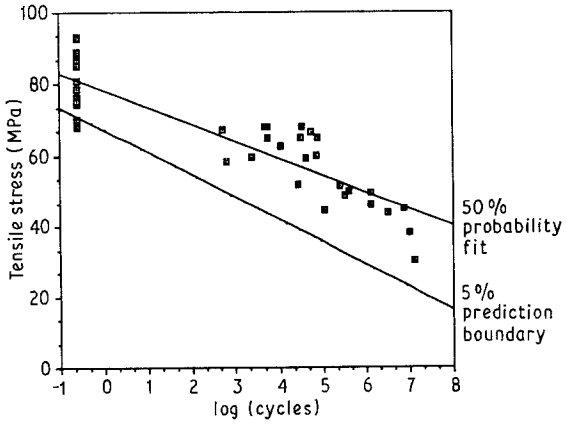

Figure 5 S–N data for Khaya at $R = 0.1$ (tension–tension) including the 5% prediction boundary.

$R = 0.1$ are plotted together in Fig. 4. Log–linear regression lines are fitted to the fatigue points as well as to the static compressive strength values at $\log_{10}N = -0.6$ (one quarter of a cycle). A sigmoidal curve fitted to the $R = -1$ data, in particular, might give a better fit, and would also suggest the existence of a fatigue limit at around 20 MPa.

As expected reversed loading at $R = -1$ is the most severe loading mode and so gives the shortest fatigue lives for a particular peak load. This is due to the stress amplitude being a maximum about a mean stress of zero so that the loading is also mixed mode. At the other R ratios, lives become progressively longer until at $R = 10$ the S–N characteristic is almost horizontal. An assesement of what constitutes failure is difficult for all compression tests at $R = 10$. For tests involving a tensile loading component failure was defined by the separation of the two halves of the sample, i.e., the formation of new surfaces, although damage could be seen to have occurred before this point. In all compression loading at $R = 10$, small compression kinks form as a test progresses but complete failure was judged to have occurred when gross cell buckling formed a compression crease across the sample. A position trip on the Mayes machine was set to stop the machine at this point.

At $R = 0.1$ (Fig. 5), for axial tension alone, the static tensile ramp test data is again plotted at $\log_{10}N = -0.6$, and has a mean value of 80.0 MPa which is significantly higher than the mean compressive strength (49.5 MPa). A 5% prediction boundary is also plotted in Fig. 5 so that an appreciation of the statistical variation in the data is obtained. Below this limit there is only a 5% probability of failure.

The transfer of S–N data to a constant-life diagram, where alternating stress is plotted versus mean stress, allows the designer to select safe combinations of alternating and mean stresses to achieve a component's design life. The S–N data from Figs 4 and 5 is combined to construct a constant-life diagram (Fig. 6) for mean fatigue lives of 10^5, 10^6 and 10^7 cycles. Alternating stress (σ_{alt}) is plotted versus mean stress (σ_{mean}) and for each life a data point relates to one S–N curve except for the limiting static strengths in tension and compression where $\sigma_{alt} = 0$. Between $R = \pm\infty$ and 1 on the left hand side of the diagram

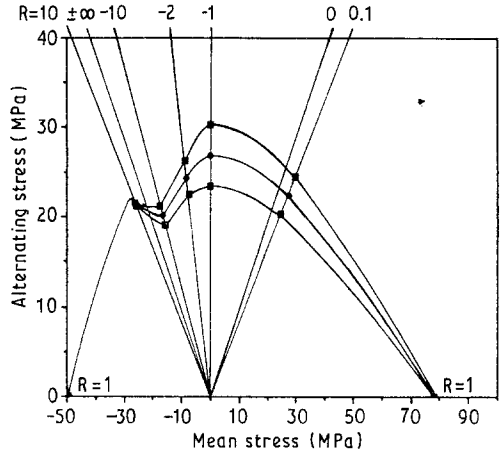

Figure 6. Constant life diagram for axially loaded Khaya.

loads are all compressive and between $R = -1$ and $\pm\infty$ loads are compressive and tensile. As the R ratio passes from -10 to $+10$ the failure mechanism changes from mixed mode to compressive. This transition is accompanied by a region of inflexion in the constant-life diagram. From Fig. 4 it can be seen that at positive R ratios in compression S–N curves will be almost horizontal so that specimen life is independent of stress. It should be noted that this curve is produced from samples that have been judged to have failed when gross buckling occurs. The $R = 10$ S–N fatigue data points all fall within the scatter of the static compressive strengths. This drives the constant-life line upwards temporarily before the decline in the alternating component of stress draws the constant-life line down to the $R = +1$ ultimate compressive strength limit. A further result of the stress independence is that points on the constant-life line for different lives coincide.

Linear Goodman relationships of the form,

$$\sigma_{alt} = \sigma_e[1 - (\sigma_{mean}/\sigma_{ult})],$$

can be drawn, where σ_e is the alternating stress at $R = -1$ and σ_{ult} is the ultimate tensile or compressive strength. The Goodman lines are constructed by joining the $R = -1$ data points to the ultimate strength points and would fall below the envelope of the constant-life lines of Fig. 6. Hence the construction of Goodman lines provides a conservative means of

simplifying the complex form of the actual constant-life lines.

The constant-life diagram indicates that although the static compression strength of Khaya is less than the tensile strength, it is ultimately the tensile fatigue properties that are likely to govern life in a turbine blade. This is because after approximately 10^7 cycles the peak stress at $R = 0.1$ (all tension) is the same as at $R = 10$ (all compression) due to the steeper gradient of the $R = 0.1$ S–N curve. After 10^7 cycles the allowable peak stress at $R = 0.1$ is less than for $R = 10$ and so, as a blade has essentially one side fatigue-loaded in tension and the other in compression, for long design lives the tensile fatigue loads are critical.

On the tensile side of the constant life diagram between $R = -1$ and 1 the behaviour is typical of that for composite materials. Fatigue properties are rarely measured in compression so the point of inflexion observed is a novel feature.

The S–N curve produced at $R = -1$ for Douglas fir is shown in Fig. 7 along with that for Khaya. There is a considerable scatter both in the static and dynamic fatigue data obtained for both species. The scatter is too great to determine whether there is a sigmoidal form to the fatigue data and hence a fatigue limit. There is a suggestion that although the Douglas fir is initially stronger in static tests its performance decreases more rapidly in fatigue.

Points on the constant-life diagrams for Khaya and Douglas fir are co-represented in Fig. 8 for lives of 10^5, 10^6 and 10^7 cycles. The diagram shows that although Douglas fir possesses superior static tensile and compressive strengths, in dynamic testing at $R = -1$ a combination of alternating and mean stresses similar to those for Khaya are obtained for each constant life. For design purposes, assuming that the data obtained for Khaya is typical of other species of wood, a straight (Goodman) line drawn between the $R = -1$ and $R = +1$ points (tension and compression) for Douglas fir should give a conservative estimate of the combinations of alternating and mean stresses which exceed a given life. Hence it is likely that only the S–N curve at $R = -1$ plus the static and compressive strengths are required to conservatively characterize constant-life lines for any wood species in axial fatigue.

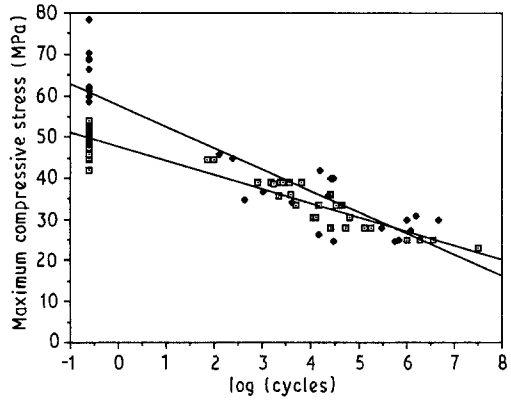

Figure 7 S–N curves for Khaya and Douglas fir at $R = -1$.

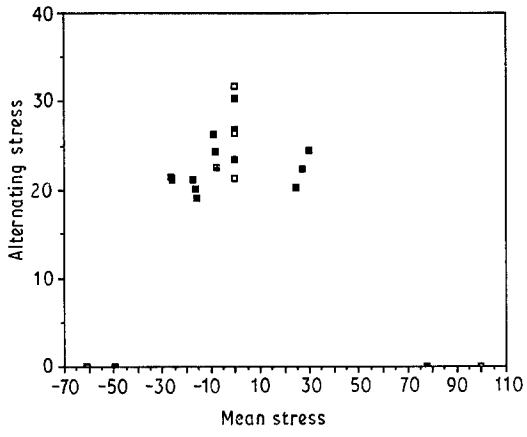

Figure 8 Outline constant life diagram for Khaya and Douglas fir at $R = -1$.

4.3. Size effect

Seventeen samples have been fatigued to failure at $R = -1$. These results are plotted with the $R = -1$ data for standard specimens in Fig. 9. The data points for the large sample are close to those for the standard samples and, if anything, lie above rather than below the line fitted to the standard data points. These fatigue results suggest that in axial tension–compression tests a size effect is not observed.

In a flexure test the stress varies continuously across the beam section, whereas in axial loading the stress distribution is close to constant. In flexure the neutral axis shifts to the tension side of the beam because the compressively loaded wood is weaker, and as the beam depth increases the beam becomes less strong. Wood is resistant to propagation of lateral cracks because of its orthotropic structure, so in pure tension or compression there is less likelihood of a size effect either in static or fatigue tests.

The failure mode of the scaled-up samples is very satisfactory. The fractured samples contain small regions of horizontally opposed compression damage linked by longitudinal tensile cracks. All the fracture surfaces lie away from the grips and testing long profiled samples is clearly advantageous.

4.4. Shear fatigue

An S–N curve (Fig. 10) has been generated at $R = 0.1$ for both the RL and TL orientations. Scatter is large

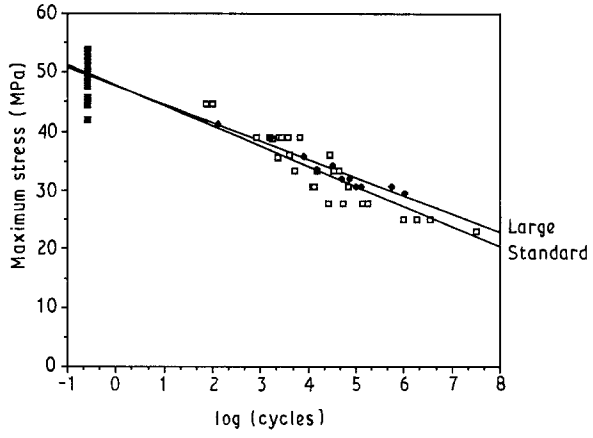

Figure 9 S–N data at $R = -1$ including results from standard and large cross-section samples.

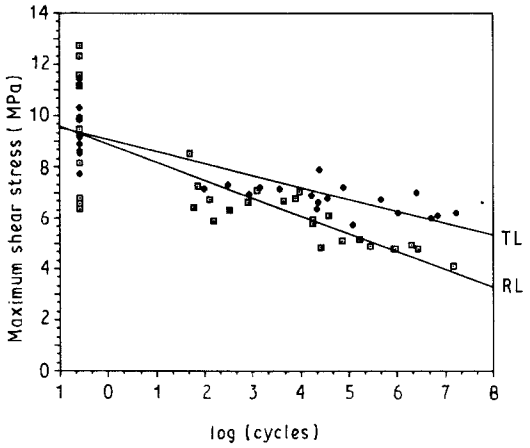

Figure 10 S–N data for Khaya in shear at $R = 0.1$.

for the static strengths, ranging from 6.4 to 12.7 MPa for the RL shear plane orientation and 7.7 to 11.4 MPa for the TL orientation. For both sample types, lives, at a given maximum stress level, span ranges of up to a maximum of three orders of magnitude, as found for axial tension–compression fatigue tests. The mean static shear strength for both TL and RL configurations is similar, so that the 50% probability of failure curve fitted to the data starts from approximately the same point. The shallower gradient of the TL 50% probability of failure curve indicates that these specimens are more resistant to shear fatigue. On the TL plane there is a requirement for longitudinal cells to cleave before failure occurs, which requires a higher shear stress than cleavage on the RL planes via planes of weak ray cells.

4.5. Fractography

4.5.1. Constant amplitude tests

An SEM examination of the fracture topography has been made at each of the five R ratios. In tension, at $R = 0.1$, crack initiation is followed by complete failure within the next few cycles of load and a large amount of longitudinal splitting is involved between small transversely cracked regions. At a cellular level (Fig. 11) there is evidence of pulled-out bunches of cells and regions of clean horizontal fracture with an absence of crushed cell ends. The large openings are vessels which allow surplus uncured resin to be removed during the vacuum bagging process.

For loading in compression at $R = 10$ heavy crushing of cell ends is observed (Fig. 12) which must occur close to the point of failure. At a macroscopic level the path of failure lies at approximately 45° to the specimen axis and gross shear-induced buckling is visible. When such buckling occurs the test is halted by the sensitive position trip.

For mixed tension/compression axial loading, at $R = -1$, -2 and -10, fracture is mixed mode and is a combination of the failures seen in Figs 11 and 12. At $R = -10$ (Fig. 13) the fracture topography is not unlike that of Fig. 12 at $R = 10$, but some cell openings are still visible. In reversed loading at $R = -1$ (Fig. 14) the fracture topography is closer to Fig. 11 and many localized areas of compression damage are

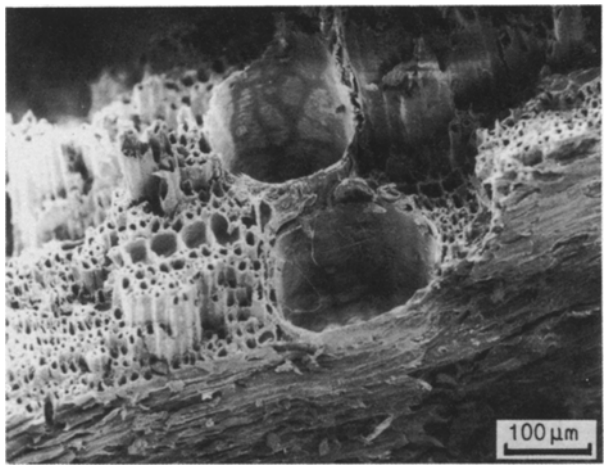

Figure 11 Stepped fracture in tension–tension at $R = 0.1$

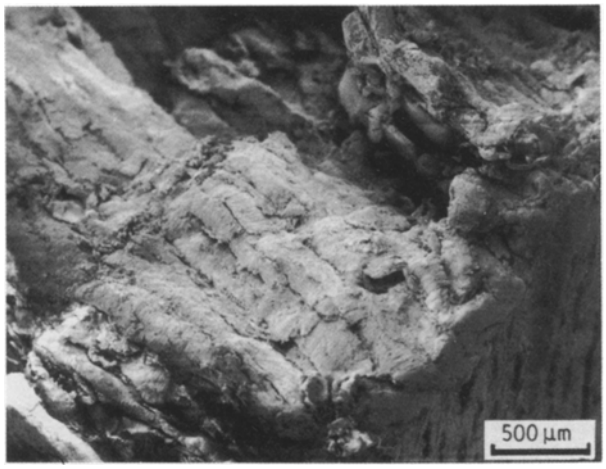

Figure 12 Compressive crushing of cell ends at $R = 10$.

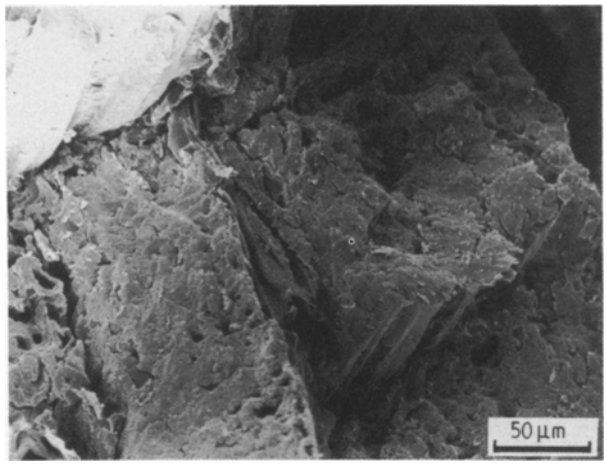

Figure 13 Fracture topography following compression–tension testing at $R = -10$.

linked by tensile cracking, so that overall, cell crushing is limited. At a higher magnification (Fig. 15) partial crushing of fibre ends is seen. When observed during test by eye, small regions of compressive rupture are visible at the sample surface at $R = -1$, often away from the edge of the sample. Longitudinal splits run

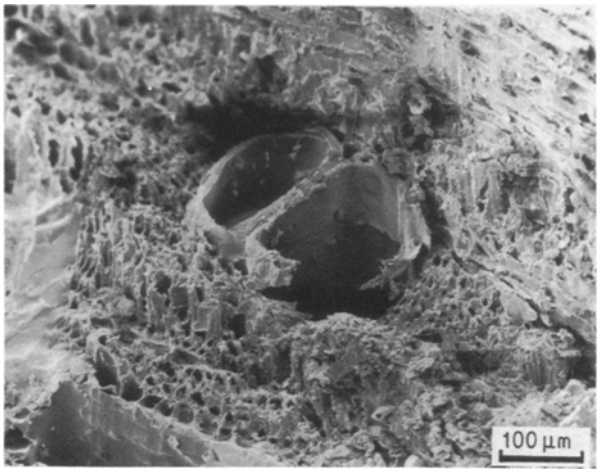

Figure 14 Cell crushing in reversed loading at $R = -1$.

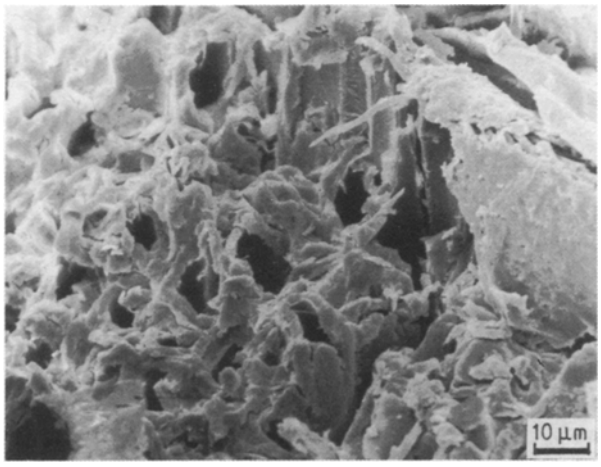

Figure 15 Partial crushing of fibre ends at $R = -1$.

from these damaged regions which frequently link other areas of localized, compressive damage.

At a cellular level compression kinking of cell walls [1] is likely to occur leading to gross cellular buckling for all R ratios other than $R = 0.1$. In tensile fatigue the higher loads will be sufficient to rupture individual weak cells leading to lateral cracking, hindered by longitudinal interfaces. This will rapidly develop into fast fracture by means of longitudinal splitting along planes of weakness such as RL planes.

4.5.2. Shear tests

In general shear failures link the ends of the horizontal cuts. As there are slight orientation differences between the grain in adjacent veneers, the shear surfaces are not completely smooth and are slightly ridged. Overall the shear failures are satisfactory and justify the choice of test geometry.

A low-magnification SEM view of shear failure in a fatigued Khaya sample, sheared along the RL plane, is shown in Fig. 16. This micrograph reveals radial planes running from left to right and longitudinal fibres and vessels running from top to bottom. The surface of the veneers is approximately TL in orientation and the fracture plane through the veneers will

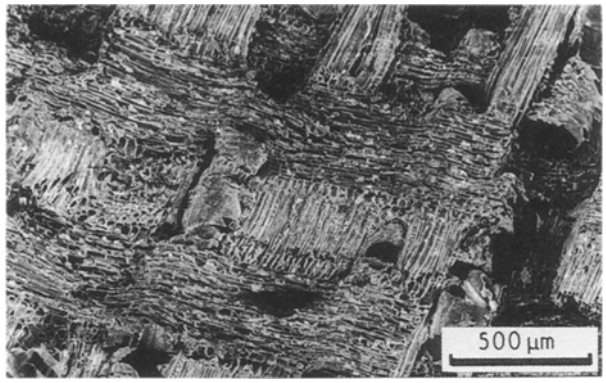

Figure 16 Shear fatigue failure across a radial–longitudinal plane.

Figure 17 Shear fatigue failure across a tangential–longitudinal plane.

thus be essentially RL. Veneers are so closely bonded in Khaya laminates that the glue lines are not easily imaged. Careful inspection of the RL cleaved plane reveals debris left behind by ruptured radial cells. The overall impression is that the radial and longitudinal elements behave as discrete structural units weakly bound together and that fracture is a rapid process resulting in little abrasive damage.

At a slightly higher magnification than Fig. 16, a general view of the fracture surface of a sample shear fatigued along the TL plane is presented in Fig. 17. The micrograph features cleanly cleaved radial cell ends and longitudinal cells that have been sheared and torn to leave a fibrous surface. The TL plane is the same plane that the glue lines run in, and some resin that has been sucked along a vessel is visible. In some samples failure occurred just adjacent to the glue lines but in all cases the wood failed rather than the resin.

4.6. General discussion

The preceding fatigue results have been generated in response to the needs of the wind-power industry which was employed laminated wood as a major material of construction for blades. To date comprehensive axial fatigue data for wood has been absent from the literature and these results partly fill this void.

The question of whether wood has a fatigue limit will only be answered by performing tests to 10^8 cycles and beyond. However there must ultimately be a

fatigue limit although it would appear to occur at a low percentage of ultimate strength.

Because of the difficulty of testing unidirectionally reinforced composites in compression fatigue, there has been very little data presented in the composites literature on the left hand side (compression/compression and tension/compression) of constant-life diagrams. The low density of wood and the greater width of wood specimens has enabled this portion of the diagram to be well characterized and it is hoped that this may promote a fuller investigation of composite systems were compression failure can be critical.

5. Conclusions

A number of conclusions relating to the axial fatigue testing of wood laminates in tension, compression and shear are summarized below.

(a) Problems associated with gripping wood laminates in axial fatigue have been overcome.

(b) Reversed loading is the most severe axial loading mode. Fatigue lives measured in all-tension tests ($R = 0.1$) are longer than those in all-compression tests ($R = 10$) because the static tensile strength of wood is much higher than the static compressive strength.

(c) S–N data at $R = 0.1, -1, -2, -10$, and 10 has yielded a set of constant life lines, the form of which is consistent with the failure mode of the wood, observed by scanning electron microscopy.

(d) The point of inflexion in constant life lines, at the R ratio where loading becomes all compressive, is a new observation, and similar effects should be observed in composite materials where failure modes are similar.

(e) An S–N curve at $R = -1$ (reversed loading) has been produced for Douglas fir/epoxy laminates. Douglas fir has a higher compressive and tensile strength than Khaya.

(f) In the constant-life diagrams for Douglas fir and Khaya, similar alternating and mean stress points appear for identical lives at $R = -1$. The general form of the diagrams is likely to be similar.

(g) Khaya/epoxy laminates have been statically and fatigue tested in shear in the RL and TL planes using a sample geometry employing displaced horizontal cuts extending a half width from opposing edges. Static tests showed that shear strength fell once the inter-cut spacing exceeded 50 mm.

(h) The shear S–N curves at $R = 0.1$ for both RL and TL orientations show large scatter. The static strengths range from 6.4 to 12.7 MPa for the RL plane and 7.7 to 11.4 MPa for the TL plane, and the fatigue lives span a maximum of three orders of magnitude for given maximum stress levels. The TL shear-fatigued samples are more fatigue resistant than the RL shear samples.

(i) Large samples with four times the cross-sectional area of the standard-sized samples have been fatigued at $R = -1$ and show no significant reduction in fatigue life at any particular maximum stress. It appears that in tension–compression the orthotropic structure of wood is insensitive to variations in the density of surface flaws.

Acknowledgement

The authors are very grateful to the UK Department of Energy for funding this work under Contract No. E/5A/CON/5046/1365.

References

1. K. T. TSAI and M. P. ANSELL, *J. Mater. Sci.* **25** (1990) 865.
2. B. MADSEN, in Proceedings of the First International Conference on Wood Fracture, Banff, Alberta (1978) p. 101.
3. J. BODIG and B. A. JAYNE, "Mechanics of wood and wood composites" (Van Nostrand Reinhold Company, USA, 1982), p. 303.
4. R. S. BARTON and W. C. LUCAS, *IEE Procs.* Pt. A, No. 9 **130** (1983) 537.
5. P. E. JOHNSON, "Design of test specimens and procedures for generating material properties of Douglas fir/epoxy laminated wood composite material with the generation of baseline data at two environmental conditions", Final Report NASA-CR-174910; DOE/NASA-0286-1; UDR-TR85-45 DEN3-286; DE-AI01-79ET-20320 850700 (1985).
6. T. STROEBEL, C. DECHOW and M. ZUTECK, "Design of an advanced wood composite rotor and development of wood composite blade technology", DOE/NASA/0260-1 NASA-CR-174713 GBI ER-11 (1984).
7. J. R. FADDOUL and T. L. SULLIVAN, "Structural fatigue test results for large wind turbine blade sections", NASA STAR Conference Paper Issue No. 09, Large horizontal wind turbines (1983) p. 303.
8. J. R. FADDOUL, "Test evaluation of a laminated wood wind turbine concept", Final report DOE/NASA/20220-30 NASA TM-81719 (1981).
9. USFPL (U.S. Forest Products Laboratory), "Wood handbook: Wood as an engineering material", U.S. Department of Agriculture Handbook 72 (1974) 4-52.
10. C. C. CHIAO, R. L. MOORE and T. T. CHIAO, *Composites* **16** (1977) 161.

Received 6 October 1989
and accepted 19 June 1990